Proceedings of the International Gas Turbine Congress 2003 Tokyo
November 2-7, 2003

IGTC2003 Tokyo TS-076

Heat Transfer in Impingement/Effusion Cooling System with Rib Turbulators

Yong Woo Nam, Dong Ho Rhee, and Hyung Hee Cho †

Department of mechanical engineering
Yonsei University
134 Shinchon-dong, Seodaemun-gu, Seoul 120-749, Korea
Phone: +82-2-2123-2828, FAX: +82-2-312-2159, E-mail: hhcho@yonsei.ac.kr

ABSTRACT

The present study is conducted to investigate the effect of rib arrangements on an impingement/effusion cooling system with crossflow. To simulate the impingement/effusion cooling system, two perforated plates are placed in parallel and staggered arrangements with a gap distance of 2 times of the hole diameter. Initial crossflow passes between the plates, and square ribs (3mm) are installed on the effusion plate. Both the injection and effusion hole diameters are 10 mm, and the flow rate of crossflow is fixed to that of the impinging jet. The Reynolds number based on the hole diameter and hole-to-hole pitch are fixed to 10,000 and 6 times of the hole diameter, respectively. To investigate the effects of rib arrangements, various rib arrangements are used. With the initial crossflow, the flow and heat/mass transfer characteristics are changed significantly from the results without the crossflow. The locally low transfer regions are formed at the mid-way between the effusion holes. Therefore, ribs were installed to obtain the uniform heat/mass transfer and to enhance the heat/mass transfer. The results present higher heat/mass transfer rates than that for a surface without ribs because the ribs prevent the wall jets from being swept away by the crossflow and increase local turbulence of the flow near the surface.

NOMENCLATURE

D	injection and effusion hole diameter
D_h	hydraulic diameter of test duct
D_{naph}	mass diffusion coefficient of naphthalene vapor in air
e	rib height
H	gap distance between injection and effusion plates
h_m	local mass transfer coefficient
I	local momentum flux ratio of crossflow and impinging jets, $\rho_c V_c^2/\rho i V_i^2$
$\dot{m}$	local naphthalene mass transfer per unit area and time
M	blowing rate (total mass flow ratio of crossflow and impinging jets), Q_c/Q_i
MR	local mass flux ratio of crossflow and impinging jets, $\rho_c Vc/\rho i Vi$
Nu	Nusselt number based on the hole diameter, hd/k
Pr	Prandtl number
P_{hole}	pitch of array holes
P_{rib}	pitch of ribs
Q_c	mass flow rate of crossflow
Q_i	mass flow rate of injected jet or effused flow
Re_d	Reynolds number based on hole diameter and the average velocity in the hole
Re_{Dh}	Reynolds number based on hydraulic diameter of duct and average velocity of crossflow
Sc	Schmidt number
Sh	Sherwood number based on the hole diameter, $h_m d/D_{naph}$
$\overline{Sh}_{sp}$	spanwise average Sherwood number
$\overline{Sh}$	overall average Sherwood number
t	thickness of injection and effusion plates
V_c	mean velocity of crossflow
V_i	mean velocity of impinging jet
w	rib width
x, z	distance from the center of a effusion hole (Fig. 2)

Greek symbols

α	rib angle of attack
ρ_c	density of crossflow
ρ_i	density of impinging jet flow
ρ_s	density of solid naphthalene
$\rho_{v,w}$	naphthalene vapor density on the surface
$\rho_{v,\infty}$	naphthalene vapor density of the injected jet.
$\Delta\tau$	test duration
Δy	local sublimation depth of naphthalene

Manuscript Received on May 13, 2003

INTRODUCTION

The thermal efficiency and specific power of gas turbine systems depend strongly on turbine inlet temperature. The inlet temperature is limited by the potential structural failure of the engine components mainly attributable to high thermal stresses and reductions in material strength due to high wall temperature. The wall temperature can be reduced by various cooling techniques such as internal convection cooling, jet impingement cooling, and film cooling. In recent years, impingement/effusion cooling, which is one of the advanced cooling schemes, has been developed and used in gas turbine engines. In this cooling scheme, the inner surfaces of hot components, such as combustor wall or blade surface, are cooled by the impingement of cooling air and outer surfaces which contact with hot gases are protected by effusion film cooling. This includes two flow situations, such as jet impingement on a plate and effusion flow through the holes of the target plate. In addition, in actual situations of combustor wall or turbine blade cooling, crossflow exists in the internal passages. Therefore, to improve cooling performance on the hot components, one should know the local heat transfer characteristics of the impingement/effusion cooling with crossflow.

The studies related to the effects of crossflow have been performed for the last few decades. Metzger and Korstad (1992) and Florschuetz et al. (1984) investigated the effects of crossflow on heat transfer/flow characteristics of array jet impingement, and reported that heat transfer is decreased at upstream region due to initial crossflow. Haiping et al. (1999) studied flow/heat transfer characteristics for impinging jets with initial crossflow in numerical method. Rhee et al. (2003) investigated the effect of crossflow on heat transfer characteristics for impingement/effusion cooling and compared with the array jet impingement with initial crossflow. They reported that the crossflow induce an adverse effect on the heat/mass transfer and the locally low transfer regions are formed when the crossflow exists. These low heat/mass transfer regions can be considered potential hot spots and the non-uniform heat transfer causes thermal stresses. Also, the overall heat/mass transfer rates on the effusion (target) plate decrease as the velocity of crossflow increases because the crossflow weakens the impingement heat transfer much more than it enhances the convective heat transfer.

In the present study, various rib arrangements are used to obtain the uniform heat/mass transfer and to enhance the heat/mass transfer for the impingement/effusion cooling with initial crossflow.

To prevent hot spots and obtain better cooling performance, not only information of overall heat transfer coefficient but also its local variation is required by Cho et al. (1997). Therefore, a naphthalene sublimation method is used to measure local heat/mass transfer coefficients on the effusion plate. This technique eliminates the conduction and radiation errors inherent in heat transfer experiments. The surface boundary condition is analogous to an isothermal surface in a corresponding heat transfer experiment.

EXPERIMENTAL APPARATUS AND PROCEDURE

Experimental Apparatus and Operating Conditions

Experimental apparatus. Figure 1 shows the schematic view of experimental apparatus. The experimental apparatus is composed of three parts; impinging jet, flow effusion and crossflow supply parts. Two inverter-controlled blowers (Blower 1 and Blower 2) are used to obtain the designed operating conditions. Blower 1 (10HP) supplies air to the impinging jet and the crossflow plenum chambers, and the flow rate through each part is controlled by gate valves. Flow in the test section (between the injection and effusion plates) is sucked through the effusion holes by Blower 2. Three orifice flow meters are installed to measure the flow rates of the crossflow, the injected jets and the effused flow. In the present study, the flow rate of the crossflow is set to be the same as the flow rate of impinging jets.

Temperature of air in each plenum chamber is measured by T-type thermocouples, and is controlled using a heat exchanger to maintain the difference between the room temperature and temperature of air in the plenums within 0.2°C. In each plenum chamber, baffles, screens and honeycombs are installed to obtain uniform flow conditions. Cho and Goldstein (1995) reported that heat/mass transfer coefficients on inside surface of the effusion plate are the same with and without crossflow over the outer surface of effusion plate (i.e. mainstream), therefore the effect of mainstream is not considered in the present study.

The crossflow duct is located between the injection and the effusion plenum chambers. Room air from Blower 1 enters the crossflow plenum chamber, and then is discharged into the room through the duct. The cross section of duct is 300 mm (W)×20 mm (H), and the hydraulic diameter (D_h) of the crossflow duct is 37.5 mm. The contraction section of which the area ratio is 6:1 is installed to obtain a uniform flow at the inlet of crossflow duct. Trip wire and sandpaper are installed to obtain a fully developed turbulent flow at the inlet region of the crossflow duct, and the distance between the inlet of duct and the first row of injection

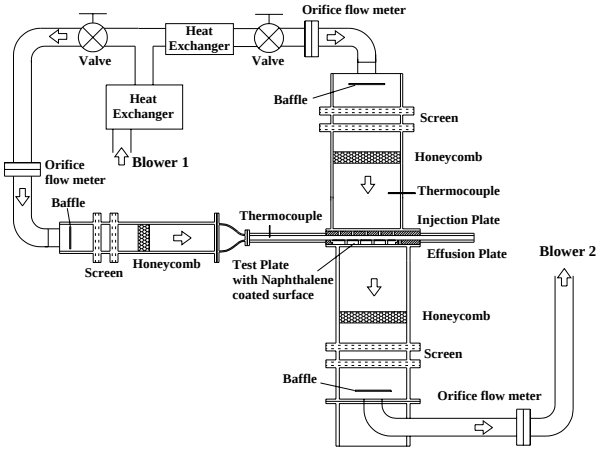

Fig. 1 Schematic view of experimental apparatus

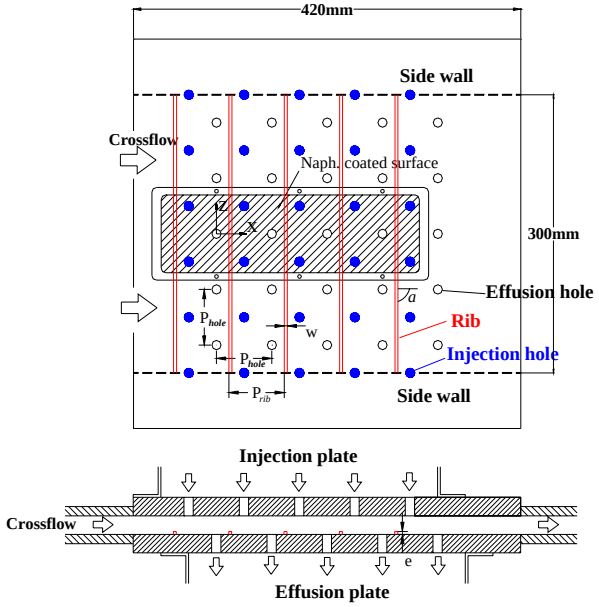

Fig. 2 Schematic diagrams of injection, effusion holes and rib arrangements

holes is set to be 400 mm (10.7 D_h).

The coordinate system and injection and effusion hole arrangements are presented in Fig. 2. The diameters of the injection and the effusion holes are 10 mm, and the thickness of plates is 20 mm (t/d=2.0). The injection and effusion plates have 25 (5×5) holes of square array, and the ratio of hole spacing to the diameter (P/d) is 6.0.

A staggered hole arrangement between the injection and the effusion plates is used in this study. The naphthalene coated test plate is installed on the effusion plate for local mass transfer measurements as shown in Fig. 2. Four effusion holes are located in the test plate and the effusion holes are protected with the aluminum rim to maintain the circular hole shapes. The naphthalene-coated area in the test plate is 8.4d×28d and T-type thermocouple is installed in the test plate to measure precisely the naphthalene surface temperature.

Rib configurations. The detailed rib configurations are illustrated in Fig. 3. The numerals of 90D, 90U, 90DU, 45V, and 45Λ represent the attack angle of the ribs. For 90D and 90U, the ribs are installed at downstream and upstream side of the effusion holes, respectively. For 90DU, the ribs are installed at both sides of the effusion holes. The case of 45V is concave and the case of 45Λ is convex toward the downstream direction (x direction) at the center line of the effusion holes.

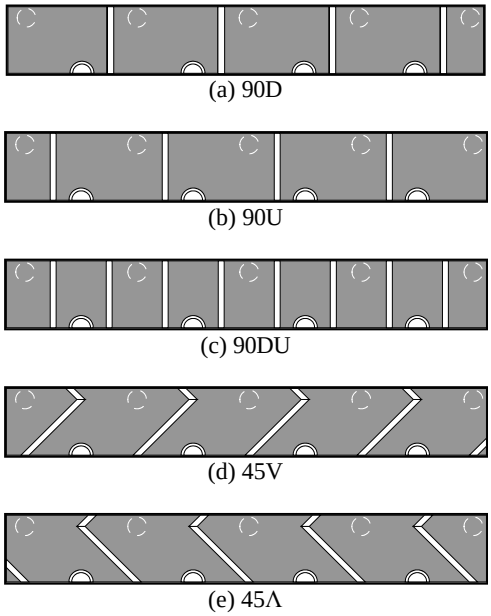

(a) 90D

(b) 90U

(c) 90DU

(d) 45V

(e) 45Λ

Fig. 3 Schematic diagrams of rib arrangements

Table. 1 Operating conditions

M	*MR*	Re_d	Re_{Dh}	*d (mm)*	D_h *(mm)*	*H/d*
1.0	0.327	10,000	12,270	10	37.5	2.0

The ribs made of aluminum have a square cross section and the rib height (*e*) and width (*w*) are 3 mm×3 mm, and the rib height-to-hydraulic diameter ratio (e/D_h) is 0.08. The ribs are glued onto the upward facing surface of the effusion plate by the double-sided tape. The rib-to-rib pitch (P_{rib}) is 60 mm so that P_{rib}/e is 20 (P_{rib} = 30 mm and P_{rib}/e = 10 for the case of 90DU).

Operating conditions. The blowing rate represents a ratio of the flow rate of the crossflow to the impinging jets, and is defined as Eq. (1).

$$M = Q_c/Q_i \tag{1}$$

The effects of the blowing rate on heat/mass transfer for the impingement/effusion cooling with crossflow are reported by Rhee et al. (2003), and in the present study, the experiments are performed with the fixed blowing rate of 1.0 (Re_{Dh}=12,270). In other words, the flow rate of the crossflow is the same as the flow rate of impinging jets. Then, the local mass flux ratio of crossflow and impinging jets (*MR*) is 0.327 and local momentum flux ratio of crossflow and impinging jets (*I*) is 0.107. The gap distance between the injection and the effusion plate is fixed at H/d=2.0. Flow rates of air through the injection holes and the effusion holes are set to be constant, and the Reynolds numbers of the flow through the injection and effusion holes are fixed at Re_d=10,000. Details of operating conditions are listed in Table 1.

Data Acquisition

In order to obtain the local mass transfer coefficients, the profile of the naphthalene surface coated on the test plate is scanned by an automated surface measuring system before and after exposure to air flow. Sublimation depth during the run is calculated from the difference of the surface profiles. The measuring system consists of a depth gauge, a linear signal conditioner (LUCAS ATA-101), a digital multimeter (Keithley model 2001), two stepping-motor driven positioners, a motor controller, and a personal computer with GPIB (IEEE-488) board. The depth gauge is a Linear Variable Differential Transformer (LVDT) made by Schaevitz Engineering (LBB-375TA-020), which has a resolution of 0.025 μm. Error of the LVDT measurements on a flat plate is less than 1% of an average sublimation depth of 40 μm during the run. The automated system typically obtains more than two thousand data points in an hour.

Heat/Mass Transfer Coefficient

The local mass transfer coefficient is defined as:

$$h_m = \frac{\dot{m}}{\rho_{v,w} - \rho_{v,\infty}} = \frac{\rho_s(\Delta y/\Delta\tau)}{\rho_{v,w}} \tag{2}$$

since incoming flow contains no naphthalene, $\rho_{v,\infty}$=0 in the present study. The naphthalene vapor pressure is obtained from a correlation of Ambrose et al. (1975). Then, the naphthalene vapor density, $\rho_{v,w}$, is calculated from the perfect gas law.

The Sherwood number can be expressed as:

$$\mathrm{Sh} = h_m d/D_{naph} \tag{3}$$

D_{naph} is based on the discussion of naphthalene properties given by Goldstein and Cho (1995). The mass transfer coefficients can be converted to the heat transfer coefficients using the heat and mass transfer analogy per Eckert (1976). Prandtl number is 0.71 for air and the Schmidt number is 2.28 for the naphthalene vapor in air at 25°C. The experiments are conducted at room temperature, and the Lewis number (Pr/Sc) for this study is about 0.307.

$$\frac{\mathrm{Nu}}{\mathrm{Sh}} = \left(\frac{\mathrm{Pr}}{\mathrm{Sc}}\right)^{0.4}, \ \mathrm{Nu} = 0.624\,\mathrm{Sh} \tag{4}$$

Uncertainty of the Sherwood numbers using the method of Kline and McClintock (1953) for single sample experiments, considering the measured temperature, depth, position and correlation equations, is within ±7.1% in the entire operating range of the measurement, based on a 95% confidence interval.

RESULTS AND DISCUSSION

In this study, the heat/mass transfer characteristics induced by the rib turbulators are investigated for the impingement/effusion cooling with initial crossflow.

Local Heat/mass Transfer

Impingement/effusion cooling with initial crossflow. Figure 4 presents the contour plot of Sh for the impingement/effusion cooling with initial crossflow. White dotted circles and the small full circles in the contour plot represent the projected positions of injection holes and the effusion holes with the aluminum rim between two circles, respectively. The local distributions of Sh for the impingement/effusion cooling with initial crossflow at z/d=3.0 and 0.0 are presented in Fig. 5.

As shown in Fig. 4, the Sherwood number contour shows a periodic distribution except the first row of injection holes because a certain amount of the crossflow and the spent air is discharged through the effusion holes and the balance between the flow entrance and exhaust is preserved. The locally high heat/mass transfer regions are formed at the stagnation regions and the regions of the high heat/mass transfer are bended and deflected toward the downstream direction by the crossflow, and the locally high heat/mass transfer coefficients are observed around the inlet of effusion holes due to the flow disturbance and the flow acceleration toward the effusion holes. However, the heart-shaped low transfer regions are formed between the effusion holes because the wall jets

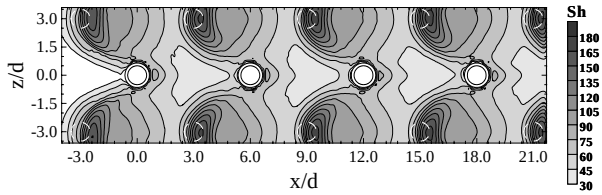

Fig. 4 Contour plot of Sh for impingement/effusion cooling with initial crossflow of blowing rate of 1.0 at Re_d=10,000 and *H/d*=2.0

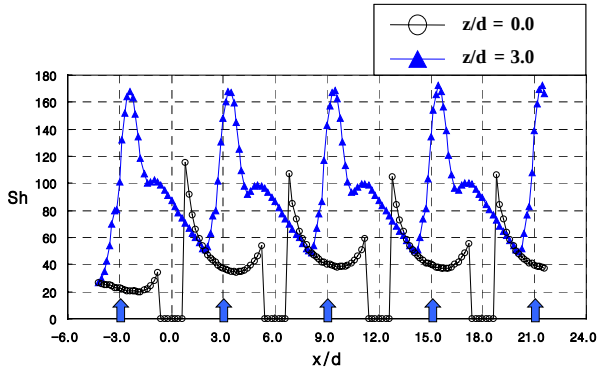

Fig. 5 Local distributions of Sh for impingement/effusion cooling with initial crossflow of blowing rate of 1.0 at Re_d=10,000 and *H/d*=2.0

swept by the crossflow are sucked by the effusion holes and the flow field is similar to that in a duct at this region.

As shown in Fig. 5, the local distributions of Sh at z/d=3.0 show that the peak values at the stagnation points increases slightly as the flow moves downstream because the interaction between the impinging jets and the crossflow enhances the turbulence intensity of jets. The secondary peaks at the downstream regions of the stagnation points appear but the peaks at the upstream region disappear. At z/d=0.0, the Sherwood numbers have peak values at the trailing edge (downstream) of the effusion holes, and then decrease monotonously. The reason is that the effusion flow through the holes removes the high concentration (temperature) air of the mass (thermal) boundary layer and the duct core flow attaches on this region. Then, the mass (thermal) boundary layer re-develops as the flow goes to the upstream side of the next effusion hole. The locally low heat/mass transfer regions are shown between the effusion holes, as mentioned before.

The low heat/mass transfer regions can be considered potential hot spots and the non-uniform heat transfer causes thermal stresses. Therefore, ribs were installed to obtain the uniform heat/mass transfer and to enhance the heat/mass transfer.

90° Ribs. Figure 6 presents the contour plots of the Sh for the 90° rib arrays; 90D, 90U, and 90DU. For the case of 90D, the stagnation regions spread a little bit toward the upstream direction because of the blockage effects of the ribs, as shown in Fig. 6(a), and the high heat/mass transfer regions around the stagnation points spread in the lateral direction because the ribs prevent wall jet from being swept away by the crossflow. Therefore, the heart-shaped low heat/mass transfer regions which are formed for the case without rib turbulator are not observed any more. The relatively high heat/mass transfer regions are observed behind the effusion holes (z/d≈0.0 and x/d≈3, 9, 15, 21) due to the promotion of the reattachment of the separation flow by the suction through the effusion holes.

For the case of 90U (Fig. 6(b)), the stagnation regions spread more than the case of 90D toward the upstream direction because of the ribs installed right behind the stagnation points and the blockage effects of the ribs. However, the low heat/mass transfer regions are formed behind the ribs (z/d≈3.0) due to the recirculation of the flows as reported by Cho et al. (2001). At the upstream

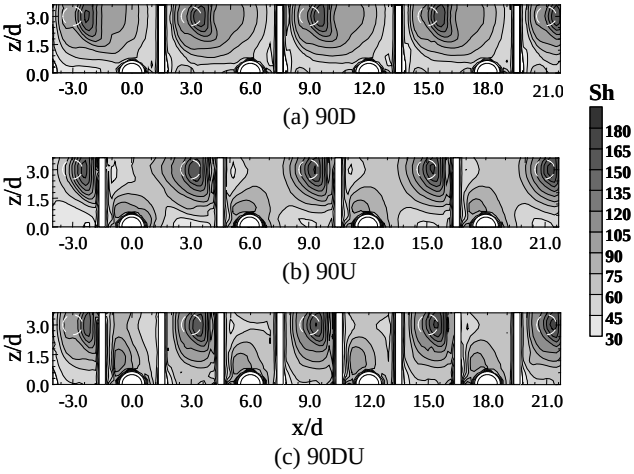

Fig. 6 Contour plots of Sh for 90° rib arrangements

regions of the effusion holes (z/d≈1.0), relatively high heat/mass transfer regions are observed due to the promotion of the reattachment of the separation flow by the suction through the effusion holes. But low heat/mass transfer regions are formed between the effusion holes (similarly the case without rib) because a certain amount of flows is effused and does not cover those regions.

For the case of 90DU (Fig. 6(c)), heat/mass transfer characteristics of 90D and 90U are observed at the same time. At the inter-rib regions where the stagnation points are formed, the stagnation regions spread a little bit toward the upstream direction because of the blockage effects of the ribs, and the high heat/mass transfer regions around the stagnation points spread in the lateral direction because the ribs prevent impinging jet from being swept away by the crossflow, like the case of 90D. At the inter-rib regions where the effusion holes exist, low heat/mass transfer regions are formed behind the rib (z/d≈3.0) due to the flow separation and recirculation, and at the upstream regions of the effusion holes (z/d≈1.0), relatively high heat/mass transfer regions are observed due to the reattachment of the separation flow, like the case of 90U.

Figures 7 and 8 present the local distributions of the Sh for the 90° rib arrays.

At *z/d*=3.0 (Fig. 7), for the cases of 90U and 90DU, locally low heat/mass transfers are shown behind the ribs due to the blockage effects of the ribs. But the case of 90D show the similar pattern with the case of no rib at *z/d*=3.0 without the locally low heat/mass transfers.

At *z/d*=0.0 (Fig. 8), for the case of 90U, locally low heat/mass transfers are shown between the effusion holes, which is not observed for the cases of 90D and 90DU, because a certain amount of flows does not cover those regions but is discharged through the effusion holes.

For the cases of 90U and 90DU, there are locally high heat/mass transfer regions before the rib which is installed after the stagnation point due to the corner vortex. But for the case of 90D, the effect of the corner vortex is not observed due to the small amount of flow as shown in Figs. 7 and 8.

V-shaped and Λ-shaped Ribs. Figure 9 shows the contour plots of the heat/mass transfer coefficients for the cases of 45V and 45Λ. The detailed local heat/mass transfer coefficients are presented in Figs. 10 and 11 for the two lateral positions (*z/d*=3.0 and *z/d*=0.0).

The V-shaped and Λ-shaped rib induce counter-rotating secondary flows, and the heat/mass transfer in the downward flow regions is augmented and that in the upward flow regions is abated as reported by Choi et al. (2002). Therefore, a complex heat/mass transfer characteristics are observed in these cases.

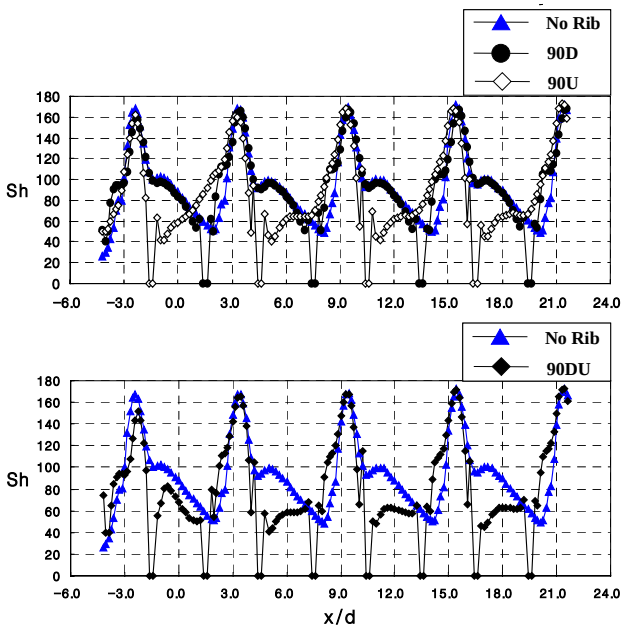

Fig. 7 Local distributions of Sh for 90° rib arrangements at z/d=3.0

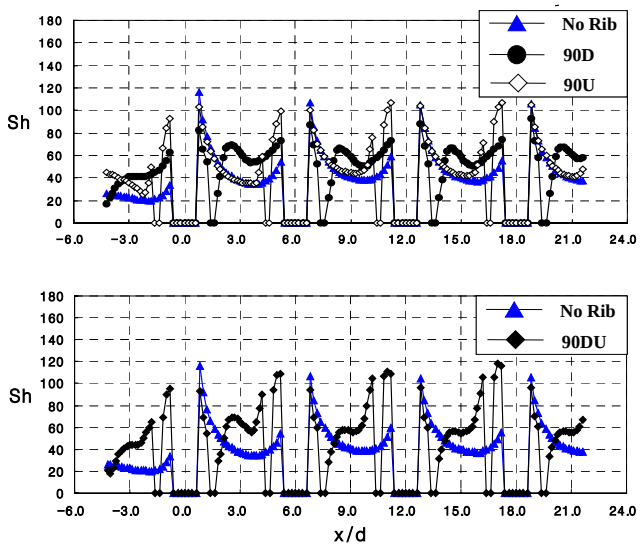

Fig. 8 Local distributions of Sh for 90° rib arrangements at z/d=0.0

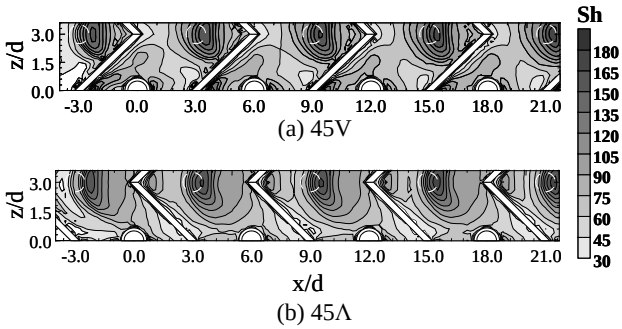

Fig. 9 Contour plots of Sh for 45° rib arrangements

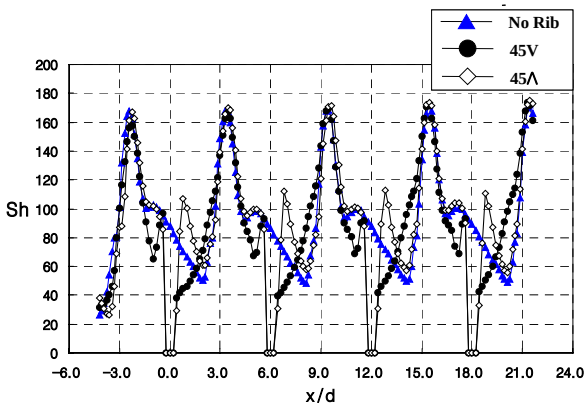

Fig. 10 Local distributions of Sh for 45° rib arrangements at z/d=3.0

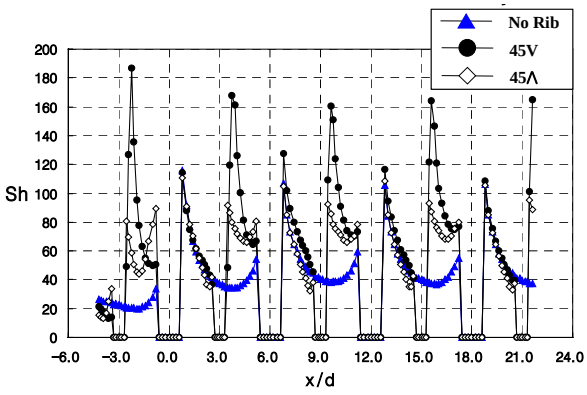

Fig. 11 Local distributions of Sh for 45° rib arrangements at z/d=0.0

As shown in Fig. 9, the secondary flows affect the heat/mass transfer distributions in the inter-rib regions. The low heat/mass transfer regions between the effusion holes are shrunk due to the secondary flows. The downward secondary flow is formed along z/d=0.0 for the case of 45V and z/d=3.0 for the case of 45Λ. The upward secondary flow is formed near the z/d=3.0 for the case of 45V and z/d=0.0 for the case of 45Λ. The heat/mass transfer in the downward flow regions is augmented. The reason is that the downward flows lead the almost naphthalene-free fluid from the mainstream and impinge onto the ribbed walls, and reinforce the flow reattachments. On the other hand, the heat/mass transfer coefficients show flat distributions without enhancement of the heat/mass transfer in the upward flow regions.

For the 45V case (Fig. 9(a)), at the upstream regions of the effusion holes, relatively high heat/mass transfer regions are observed due to the downward secondary flows, which is reinforced by the flow suction through the effusion holes (like the case of 90U).

For the case of 45Λ (Fig. 9(b)), relatively high heat/mass transfer regions are observed before the effusion holes (z/d≈0.0 and x/d≈4, 10, 16) due to the promotion of the reattachment of the separation flow by the suction through the effusion holes. But, low heat/mass transfer regions are formed behind the effusion holes (z/d≈0.0 and x/d≈2, 8, 14, 20) because of the upward secondary flows and the flow suction.

As shown in Fig. 10, at the stagnation points, all three cases have the almost same values. For the case of 45V, the secondary peaks of heat/mass transfer coefficients are observed in front of the ribs in spite of the upward flow regions. The reason is that the corner vortices are formed and the impinging jets weaken the effects of the upward flows at these regions. But the locally low heat/mass transfers are shown behind the ribs due to the recirculation of the flows. For the case of 45Λ, the locally high heat/mass transfers are shown behind the ribs due to downward secondary flows.

At z/d=0.0 (Fig. 11), for the case of 45V, the peaks are not observed in front of the ribs because a certain amount of flows is effused and does not cover those regions. But the locally high heat/mass transfers are shown behind the ribs at the downward flow regions and these values are much higher than the values for the case of 45Λ (Fig. 10) because the downward flows are strengthened by the

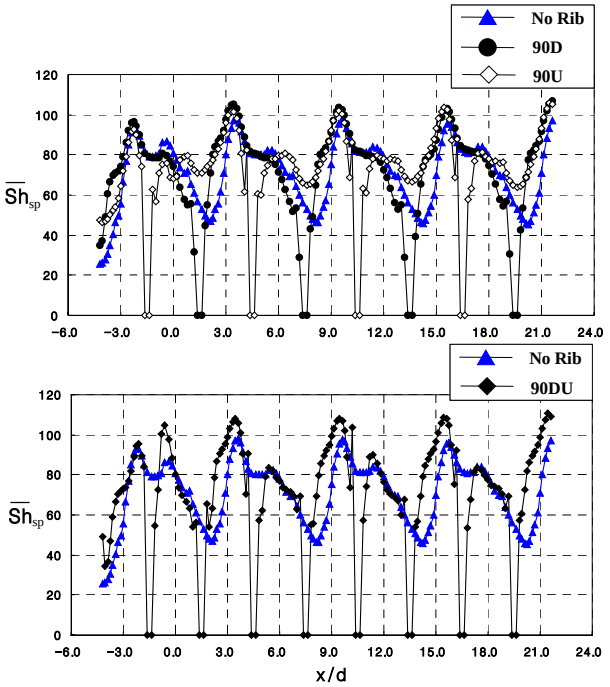

Fig. 12 Spanwise averaged Sh for 90° rib arrangements

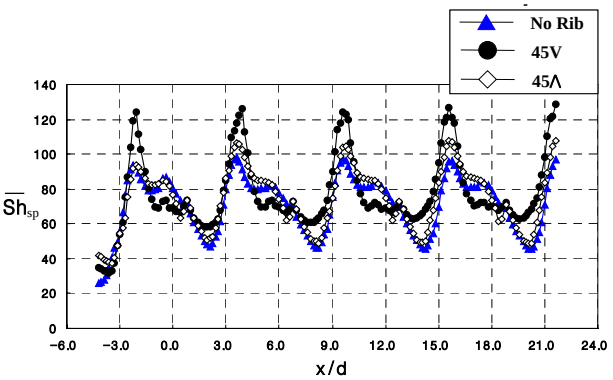

Fig. 13 Spanwise averaged Sh for 45° rib arrangements

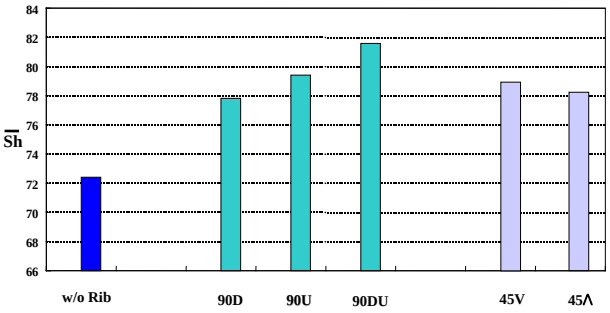

Fig. 14 Overall averaged Sh for various rib configurations at M=1.0, Re_d=10,000, and H/d=2.0.

flow suction for 45V case, as mentioned above. For the case of 45Λ, the secondary peaks of high heat/mass transfer can not observed in front of the ribs because of the upward secondary flows.

Average heat/mass transfer. Figures 12 and 13 present the spanwise averaged Sherwood numbers on the effusion plate for the various rib arrangements. The averaged values are obtained by taking the local data in the region of $0.0 \le z/d \le 3.0$. The average Sherwood numbers for 90U show the most uniform values for all the tested cases due to the promotion of the reattachment of the separation flow by the flow suction around the effusion holes. But for the case of 90U as shown in Figs. 6(b) and 8, there are locally low heat/mass transfer regions between the effusion holes and behind the ribs ($z/d \approx 3.0$).

For the case of 90DU, high average Sherwood numbers are observed at the inter-rib regions where the stagnation points are formed. But, relatively low average Sherwood numbers are observed at the inter-rib regions where the effusion holes exist. This pattern is periodic except the first row of injection and effusion holes.

Figure 13 presents the spanwise averaged Sherwood numbers on the effusion plate for the cases of 45V and 45Λ. For the case of 45V, the average values at the stagnation points are about 30% higher than those for the case of 45Λ. The reason is that the high transfer regions due to the downward secondary flows are formed at the same lateral positions as stagnation regions.

For the case of 45Λ, the secondary peaks of the spanwise averaged Sherwood numbers are observed at $x/d \approx 1$, 7, 13, and 19 because of the downward secondary flows. The lowest spanwise averaged Sherwood numbers are observed between the effusion hole region and the stagnation region ($x/d \approx 2$, 8, 14, 20) because of the flow suction through the effusion holes and the upward secondary flows.

Figure 14 shows the overall averaged Sherwood numbers on the effusion plate for various cooling schemes. The overall averaged values are obtained by taking the local data in the region of $0.0 \le z/d \le 3.0$ and $0.0 \le x/d \le 18.0$. For all the tested cases, the cooling performances are better than that of the impingement/effusion cooling with initial crossflow (without rib). The case of 90DU shows about 12% higher cooling performance than the impingement/effusion cooling with initial crossflow (without rib). The case of 90U shows a little bit higher cooling performance than the case of 90D. The average cooling performances for the cases of 45V and 45Λ are almost the same.

CONCLUSIONS

In the present study, the heat/mass transfer characteristics induced by the rib turbulators for the impingement/ effusion cooling with initial crossflow are investigated and compared with those for the impingement/effusion cooling with initial crossflow (without rib turbulator). The results are summarized as follows:

- With the initial crossflow (without rib), the regions of high heat/mass transfer at the stagnation points are bended and deflected toward the downstream direction by the crossflow, and the heart-shaped low heat/mass transfer regions are formed between the effusion holes because the wall jets swept by the crossflow are sucked by the effusion holes.
- All the cases with the rib turbulators show better cooling performances than that of the impingement/effusion cooling without rib and the heart-shaped low heat/mass transfer regions for the impingement/effusion cooling with initial crossflow (without rib) disappear by installing the rib turbulators.
- For the 90° rib arrays, the stagnation regions spread toward the upstream direction because of the blockage effects of the ribs and the high heat/mass transfer regions around the stagnation points spread in the lateral direction because the ribs prevent wall jet from being swept away by the crossflow. The average cooling performance for the case of 90U shows a little bit higher than that for the case of 90D. For the case of 90DU, heat/mass transfer characteristics of 90D and 90U are observed at the same time. The average cooling performance for 90DU shows the highest value for all the tested cases and that is about 12% higher than the impingement/effusion cooling with initial crossflow (without rib).
- The V-shaped and Λ-shaped rib induce counter-rotating secondary flows. Therefore, a complex heat/mass transfer characteristics are observed in these cases. The heat/mass transfer in the downward flow regions is augmented and that in the upward flow regions is abated. For the case of 45V, the heat/mass transfer in the downward flow regions is much higher than that for the case of 45Λ because the downward flows are strengthened by the flow

suction for 45V case. But the average cooling performances for the cases of 45V and 45Λ are almost the same, in spite of the difference of the rib arrangements.

ACKNOWLEDGMENTS

The authors wish to acknowledge support for this study by Ministry of Science and Technology through National Research Laboratory program.

REFERENCES

Ambrose, D., Lawrenson, I. J. and Sparke, C. H. S., 1975, "The Vapor Pressure of Naphthalene," J. Chem. Thermo., **7**, pp. 1173-1176.

Cho, H. H. and Goldstein, R. J., 1995, "Heat (Mass) Transfer and Film Cooling Effectiveness with Injection through Discrete Holes – Part I: within holes and on the back surface," J. of Turbomachinery, **117**, pp. 440-450.

Cho, H. H. and Goldstein, R. J., 1996, "Effect of Hole Arrangements on Impingement/ Effusion Cooling," *Proceeding of the 3rd KSME-JSME Thermal Engineering Conference*, pp. 71-76.

Cho, H. H., Lee, C. H. and Kim, Y. S., 1997, "Characteristics of Heat Transfer in Impinging jets by Control of Vortex Pairing," *ASME Paper* No. 97-GT-276.

Cho, H. H. and Goldstein, R. J., 1997, "Total Coverage Discrete Hole Wall Cooling," *J. of Turbomachinery*, **119**, No. 2, pp. 320-329.

Cho, H. H., Wu, S. J. and Kwon, H. J., 2000, "Local Heat/Mass Transfer Measurements in a Rectangular Duct with Discrete Ribs," *ASME Journal of Turbomachinery*, Vol. 122, pp. 579-586.

Cho, H. H., Yoon, P. H. and Rhee, D. H., 2001, "Heat/mass transfer characteristics of arrays of impingement jets with effusion holes", *Proceedings of ExHFT-5*, pp. 955-960

Cho, H. H. and Rhee, D. H., 2001, "Local Heat/Mass Transfer Measurement on the Effusion Plate in Impingement/Effusion Cooling System," *J. of Turbomachinery*, **123**, pp. 601-608.

Cho, H. H., Choi, J. H. and Rhee, D. H. 2001, "The effects of hole arrangements on heat/mass transfer of impingement/effusion cooling system", *Proceedings of ExHFT-5*, pp. 975-980.

Cho, H. H., Lee, S. Y. and Wu, S. J., 2001, "The Combined Effects of Rib Arrangements and Discrete Ribs on Local Heat/Mass Transfer in a Square Duct," ASME Paper No. 2001-GT-0175.

Choi, C., Rhee, D. H. and Cho, H. H., 2002, "Heat/Mass Transfer and Pressure Drop in A Square Duct with V-Shaped Ribs," *KSME journal* B, Vol. 26, No. 11, pp. 1542-1551.

Dittus, P. W. and Boelter, L. M. K., 1930, Univ. Cal. Pebl. Engng, **2**(13), pp. 443-461; 1985 reprinted in *Int. Commun. Heat Transfer*, **12**, pp. 3-22.

Eckert, E. R. G., 1976, Analogies to Heat Transfer Processes, in Measurements in Heat Transfer, ed. Eckert, E. R. G. and Goldstein, R. J., pp. 397-423, Hemisphere Pub., New York.

Florschuetz, L. W., Metzger, D. E. and Su, C. C., 1984, "Heat Transfer Characteristics for Jet Array Impingement With Initial Crossflow," *J. of Heat Transfer*, **106**, pp. 34-41.

Goldstein, R. J. and Cho, H. H., 1995, "A Review of Mass Transfer Measurement Using Naphthalene Sublimation," *Experimental Thermal and Fluid Science*, **10**, pp. 416-434.

Goldstein, R. J., Cho, H. H. and Jabbari, M. Y., 1997, "Effect of Plenum Crossflow on Heat (Mass) Transfer Near and Within the Entrance of Film Cooling Holes," *J. of Turbomachinery*, **119**, pp. 761-769.

Hollwarth, B. R. and Dagan, L., 1980, "Arrays of Impinging Jets with Spent Fluid Removal through Vent Holes on the Target Surface Part 1: Average Heat Transfer," *J. of Engineering for Power*, **102**, pp. 994-999.

Hollwarth, B. R. and Lehmann, G. and Rosiczkowski, J., 1983, "Arrays of Impinging Jets with Spent Fluid Removal through Vent Holes on the Target Surface Part 2: Local Heat Transfer," *J. of Engineering for Power*, **105**, pp. 393-402.

Haiping, C., Wanbing, C. and Taiping, H., 1999, "3-D Numerical Simulation of Impinging Jet Cooling with Initial Crossflow," *ASME Paper* No. 99-GT-256.

Kline, S. J. and McClintock, F., 1953, "Describing Uncertainty in Single Sample Experiments," *Mech. Engineering*, **75**, p. 3-8.

Lee, J. H. and Lee, S. J., 1998, "Turbulent Heat Transfer Characteristics in a Stagnation Region of Axi-Symmetric Jet Impingement," *Proceedings of 11th IHTC*, **5**, pp. 433-438.

Metzger, D. E. and Korstad, R. J., 1992, "Effects of Cross flow in Impingement Heat Transfer," *J. of Engineering for Power*, **94**, pp. 35-41.

Rhee, D. H., Choi, J. H. and Cho, H. H., 2003, "Flow and Heat(Mass) Transfer Characteristics in an Impingement/Effusion Cooling System with Crossflow," *J. of Turbomachinery*, **125**, No. 1, pp. 74-82.